Journal Pre-proof

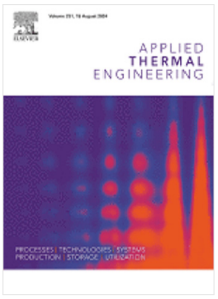

Addressing multi-step inverse heat transfer problems via reduced order models in a cooling process for polymer pipes with sparse measurements

Raphael Hartner, Martin Kozek, Stefan Jakubek

PII: S1359-4311(24)02151-3
DOI: https://doi.org/10.1016/j.applthermaleng.2024.124483
Reference: ATE 124483

To appear in: *Applied Thermal Engineering*

Received date : 3 December 2023
Revised date : 14 September 2024
Accepted date : 24 September 2024

Please cite this article as: R. Hartner, M. Kozek and S. Jakubek, Addressing multi-step inverse heat transfer problems via reduced order models in a cooling process for polymer pipes with sparse measurements, *Applied Thermal Engineering* (2024), doi: https://doi.org/10.1016/j.applthermaleng.2024.124483.

Addressing Multi-Step Inverse Heat Transfer Problems via Reduced Order Models in a Cooling Process for Polymer Pipes with Sparse Measurements

Raphael Hartner[a], Martin Kozek[b], Stefan Jakubek[b]

[a]*Institute of Industrial Management, University of Applied Sciences JOANNEUM, Kapfenberg, 8605, Austria*
[b]*Institute of Mechanics and Mechatronics, Vienna University of Technology, Vienna, 1060, Austria*

Abstract

In modern polymer pipe extrusion processes with connected post-processing steps, the intermediate cooling and conditioning process is essential for the resulting product quality. In such cases, computationally efficient models are required for real-time process control and optimization. Unfortunately, heat transfer coefficients are rarely known for actual production processes, leading to an inverse heat transfer problem. Existing methods mainly rely on computationally intensive numerical models or on data intensive neural networks. Both are not suitable, if only sparse measurements are available and a fast execution time is required. In contrast to that, we propose to use a proper orthogonal decomposition and project the governing heat equation onto extracted basis functions via the Galerkin method. This leads to an efficient and accurate reduced order model, which can be used for parameter identification and subsequent process control. Regarding the identification, we address the ill-posed problem with well-known relative constraints, l_2 regularization and decomposition of coefficients based on the Nusselt number. Simulation and experimental results show that the heat transfer coefficients are consistently identified and robust against initial parameter guesses despite sparse and noisy temperature measurements. Consequently, the proposed method can be efficiently applied in cooling and conditioning processes in polymer extrusion and related applications such as identifying the heat transfer coefficients and thermal resistance in pressurized surge lines of nuclear power plants and brick walls in melting furnaces respectively.

Keywords: reduced order model, proper orthogonal decomposition, inverse heat transfer problem, pipe extrusion, nonlinear parameter identification, constrained identification

1. Introduction

Modern polymer extrusion processes are often equipped with directly connected post-processing steps, for instance pipe drawing to improve its mechanical properties through oriented polymer chains [1, 2]. In such cases, the intermediate cooling and conditioning steps are essential for achieving high product quality, whereas efficient and accurate models are required for real-time process control and optimization. These models need to cope with nonlinear process behavior, multiple connected process steps with long transport delays [3] and the governing heat equation to extrapolate beyond simple stationary operating points.

However, boundary conditions and their heat transfer coefficients for each cooling and conditioning process step are usually unknown for actual production lines, leading to an inverse heat transfer problem (IHTP), which is inherently difficult to solve due to its ill-posed nature. To address this problem, several research directions arose and were further developed in recent years [4].

Neural networks are used as surrogate models of the system to solve different variations of the IHTP, where the main advantage is their fast inference allowing it to be applied in real-time applications. Billah et al. [5] used physics-informed neural networks (PINN) to solve the IHTP for 1D domains, where unknown properties are defined as trainable parameters and simultaneously identified during the training process. In this regard, the governing equations are built into the PINN as regularization to improve its extrapolation capabilities. Similarly, Cai et al. [6] developed a PINN to estimate the temperature and velocity field in a 2D convective domain. As before, unknown properties were identified during the training process. Another approach to use neural networks in IHTPs was introduced by Gu et al. [7], where a generative adversarial network (GAN) was trained to inversely identify transient heat fluxes in pool boiling processes. Even though the underlying governing equations were not built into the neural network directly, the model showed good results and fast execution times.

In spite of requiring only a few measurement points in the spatial domain, aforementioned methods require continuous temperature measurements in time. Therefore, these methods are hardly suitable for actual cooling and conditioning process steps, where sparse sensor locations and a Lagrangian view of the process, meaning a cross section of the moving pipe is followed through the line, lead to sparse measurements in the time domain.

In contrast to neural networks, conventional methods employ a parameterized forward model, for instance based

on finite element (FE), finite difference (FD) or finite volume (FV), and an optimization algorithm to identify unknown parameters or boundary conditions of the model [4]. Duda [8] proposed a general method based on an FE direct model and the Levenberg-Marquardt optimization algorithm to identify boundary heat fluxes in heating processes based on simulated temperature measurements. Similarly, Reddy et al. [9] generally reviewed benefits and drawbacks of FE models for inverse problems and found that direct models based on FE are well suited for IHTP due to their flexibility. As a result, the combined method of a numerical direct model and an optimization algorithm to solve IHTPs is widely applied in several domains.

Lu et al. [10] applied the conjugate gradient method based on an FE model of pressurized surge lines in a nuclear power plant to identify the convective heat transfer coefficient as well as fluid and inner wall temperatures solely based on temperature measurements on the outside. Bozzoli et al. [11] employed a numerical model of a coiled tube to estimate the local convective wall heat flux using experimental data. The ill-posed problem was addressed by Tikhonov regularization and fixed-point iteration to select suitable regularization weights. Palumbo et al. [12] focused on identifying the interfacial heat transfer coefficient in sand mold casting processes. For that purpose, a genetic algorithm was used to fit the direct FD model on experimental temperature measurements. Similarly, Udayraj [13] analyzed the effectiveness of three metaheuristic algorithms – ant colony optimization (ACO), cuckoo search and particle swarm optimization – in different settings, and found that the ACO is most effective to reconstruct the heat flux based on temperature measurements. Noh et al. [14] utilized a thermal resistance network as direct model in combination with a Kalman filter and a recursive least-squares algorithm to determine the heat flux in gun barrels based on experimental temperature measurements on the outer surface. Moreover, Hafid and Lacroix [15] utilized an FV model to identify the heat flux and thermal resistance of the brick wall in a melting furnace. To improve the computational efficiency of the identification process the Levenberg-Marquardt algorithm was extended with the Broyden-method. Additionally, the influence of measurement noise was investigated. Gostimirovic et al. [16] employed an FE model with the conjugate gradient method to identify the heat flux in grinding processes, which is used to optimize the process parameters.

As shown by the literature, numerical methods are often used as direct model while an optimization algorithm fits the parameters of the model to simulated or experimentally measured data. However, the resulting direct models are computationally intensive and hardly suitable for real-time application in process control and optimization. Additionally, most identification procedures require continuous temperature measurements in time, which is difficult to accomplish in cooling and conditioning processes with moving goods, multiple process steps and an Lagrangian view on the system.

Even though numerical models can be systematically optimized to reduce the degrees of freedom [17] and consequently, improve computational efficiency, their applicability is still limited where fast execution times are required. In such cases, reduced order models (ROM), based on the Galerkin method and optimal basis functions extracted via proper orthogonal decomposition (POD), can reduce the degrees of freedom (DOF) and computational effort by several orders of magnitude.

Star et al. [18] applied the POD-Galerkin method for a turbulent convective buoyant flow, where the data used for extracting the POD modes were generated by an FV model with varying parameters to cover an appropriate range. After extracting POD modes for velocity, pressure and temperature and projecting the governing equation, it was found that the execution time for simulation runs can be reduced by a factor of 10^5 while maintaining acceptable accuracy. Additionally, in spite of its linear characteristic, the ROM covers the nonlinearity of the system to a high degree. Similarly, Escanciano and Class [19] applied the POD-Galerkin method to develop a ROM of a deep water pool for storing nuclear material. The snapshots for computing the POD modes were generated by a computational fluid dynamics (CFD) model. Since the ROM requires only a fraction of the computational efforts, parameter spaces can be efficiently explored to determine safe operating conditions. Additionally, since simulating the heat transfer processes in CPUs requires lightweight models with few DOF, Jiang et al. [20] developed a ROM based on the POD-Galerkin method, where the input data for extracting the modes were generated by an FE model. Importantly, the parameters of the high-fidelity simulation were chosen to cover a physically feasible range to ensure that the ROM is capable of representing a wide range of scenarios. Identical to aforementioned research, the computational efforts were reduced by several orders of magnitude.

As a result, due to its significant computational advantage in comparison to high-fidelity full order models, ROMs based on Galerkin-POD are also well suited for IHTP. Park et al. [21] used a high-fidelity FD model with varying parameters to extract meaningful modes. After projecting the heat equation, the ROM was used as forward model to identify transient heat sources in a 2D solid body with temperature dependent heat conductivity through the conjugate gradient method. As a result, the computation time was significantly reduced while maintaining high accuracy in comparison to the high-fidelity FD model. Moreover, Pham et al. [22] applied the POD-Galerkin method to a 1D IHTP of a solid wall to identify the unknown thermal diffusivity. In contrast to the aforementioned source, the Levenberg-Marquardt optimization algorithm was applied to fit the forward model to simulated temperature measurements. Interestingly, only one virtual sensor was sufficient to accurately identify the thermal diffusivity in spite of added random noise.

As shown, reduced order models were successfully ap-

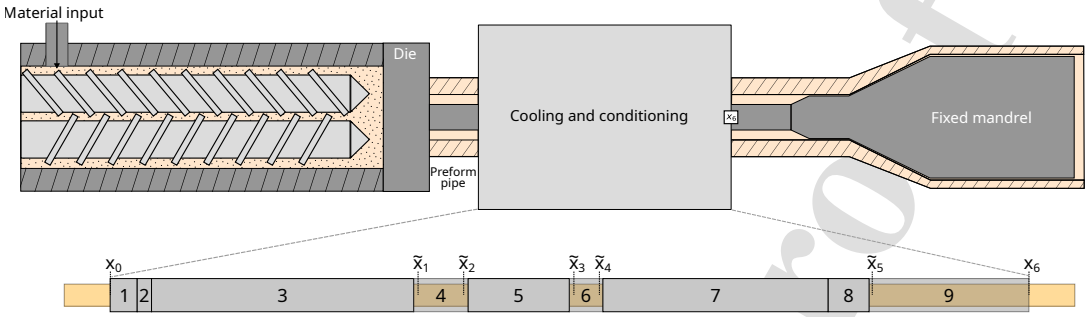

Figure 1: Pipe extrusion process with directly connected drawing process and intermediate cooling and conditioning steps (top view), where manual and automated temperature measurements are indicated by $\tilde{x}_k$ and x_k respectively.

plied to model heat and mass transfer processes for both, pure simulation purposes and as forward model for IHTP. However, to the best of our knowledge, neither high-fidelity models nor ROMs were employed in multi-step cooling and conditioning processes where multiple heat transfer coefficients need to be identified simultaneously. Additionally, all related work require continuously measured temperature in the time domain, which cannot be achieved when a Lagrangian view of the system is considered. Therefore, we propose to use a proper orthogonal decomposition based on simulation data and project the governing heat equation on the extracted basis functions. This ROM is then used to efficiently solve the IHTP and consistently identify the heat transfer coefficients while making use of well-known relative constraints and l_2 regularization to address its ill-posed nature. Furthermore, to account for multiple product dimensions, the optimization problem is formulated in terms of Nusselt number and characteristic length, which reduces the number of unknown parameters significantly. As a consequence, the novelty of this work and the main contributions can be summarized as follows:

- Develop a reduced order model of a multi-step cooling and conditioning process to increase computational efficiency while maintaining accuracy.
- Formulate the optimization problem based on Nusselt number and characteristic length to reduce the number of unknown parameters.
- Address the ill-posed nature through l_2 regularization and well-known relative constraints.
- Solve the IHTP for multi-step cooling and conditioning processes with multiple product dimensions in spite of sparse temperature measurements in time.
- Validate the proposed method with simulated and experimental data.

Importantly, the proposed methodology is generically applicable for polymer extrusion and related problems, such as identifying the heat transfer coefficients in pressurized surge lines of nuclear power plants and the thermal resistance of brick walls in melting furnaces.

This paper is structured as follows. Section 2 describes the production process with its cooling and conditioning steps as well as the governing heat equation. Section 3 elaborates on the proposed methodology based on proper orthogonal decomposition, Galerkin method and parameter identification with relative constraints and regularization. Section 4 and 5 include the results based on simulated and experimental data respectively. The results and its limitations are discussed in section 6, whereas section 7 concludes this paper.

2. Problem Formulation

2.1. Process and Material Specification

Modern pipe production lines are often equipped with directly connected post-processing steps. In the case of bi-oriented PVC pipe production, the temperature profile of the pipe is essential for the quality of the drawing process. As shown in Fig. 1, a twin-screw extruder produces a melt with consistent quality, which is formed by the die head to a preform pipe. Several cooling and conditioning steps determine the temperature profile at the drawing process, where a fixed mandrel is used to enlarge the preform diameter (circumferential orientation). Additionally, the increased pipe speed after the drawing process, controlled by haul-offs, stretches the pipe in length, leading to an axial orientation of the polymer chains.

The specific production line which is used to develop and validate the methods consists of 9 cooling and conditioning steps with varying lengths (see Fig. 1) where forced and mixed convection of water and air are involved. As described in Table 1, within three steps the pipe is in contact with ambient air where mixed convection is assumed. In the other steps, the pipe is shielded from the environment and subject to forced convection either through spray cooling (see Fig. 2), immersion cooling or fanned air

Figure 2: Active spray cooling in process step 1 as an example of forced convection with water as coolant.

Step	Type	Convection	Fluid
1	Spray Cooling	Forced	Water
2	Immersion Cooling	Forced	Water
3	Spray Cooling	Forced	Water
4	Ambient Air	Mixed	Air
5	Spray Cooling	Forced	Water
6	Ambient Air	Mixed	Air
7	Conditioning	Forced	Air
8	Spray Cooling	Forced	Water
9	Ambient Air	Mixed	Air

Table 1: Details of the cooling and conditioning steps for the underlying pipe extrusion line.

conditioning. At the end of these steps, an infrared temperature sensor is mounted above the moving pipe at x_6. Apart from that, a thermocouple sensor is located after the extruder within the die head to measure the melt temperature. Consequently, only sparse information is available for the identification process. However, since the components 4, 6 and 9 are partially open, manual measurements can be performed within these steps indicated by $\tilde{x}_k$ to facilitate the identification.

In addition to multiple cooling and conditioning steps, different pipe dimensions can be produced in the same production line. These products have different diameters, wall thicknesses and production speeds, while the material (PVC) remains the same. As a result, the cooling effect on the pipe differs among different dimensions, leading to 9 unknown heat transfer coefficients for each pipe dimension which must be identified with sparse measurements.

2.2. Direct Model

To model the cooling and conditioning process, a Lagrangian view is used, meaning that one cross-section of the pipe is followed through the line at a time. Additionally, assuming homogeneous boundary conditions along the circumference reduces the problem domain to one slice of the cross-section moving through the line. Consequently, the one-dimensional transient heat equation in polar coordinates is considered as governing equation.

$$\frac{\partial u}{\partial t} - \frac{\alpha(u)}{r}\left(\frac{\partial u}{\partial r} + r\frac{\partial^2 u}{\partial r^2}\right) = 0 \tag{1}$$

The temperature is a function of time t and radius r and denoted by $u = u(r, t)$. The radial heat transfer within the pipe wall is determined by the temperature dependent thermal diffusivity $\alpha(u)$ which is a function of material properties, namely thermal conductivity λ_s, material density ρ and specific heat capacity c_p.

$$\alpha(u) = \frac{\lambda_s}{\rho c_p(u)} \tag{2}$$

In the case of PVC, c_p has a nonlinear dependency on temperature whereas this relationship is usually experimentally assessed and available in diagrams, particularly for temperatures above the glass transition temperature and therefore, above its operating range. Consequently, the temperature dependency as provided in [23] is approximated with the following logistic function.

$$c_p(u) = 920 + 2.4u + \frac{300}{1 + e^{-(u-75)}} \tag{3}$$

The initial condition for the direct model is assumed to be homogeneous from inner r_{in} to outer radius r_{out}, which are defined by the specific pipe dimension.

$$\text{IC: } u(r, t = 0) = u_0 = \text{const}, \; r \in [r_{in}, r_{out}] \tag{4}$$

The radial domain of the heat equation requires two boundary conditions. On one hand, since the center of the pipe is filled with air, which is neither cooled nor fanned and has a significantly lower specific heat capacity than PVC, the influence is negligible. Therefore, an adiabatic Neumann condition is specified on the inner pipe surface.

$$\text{BC1: } \frac{\partial u}{\partial r} = 0, \text{ at } r = r_{in} \tag{5}$$

On the other hand, the outer surface of the pipe is subject to a convective (Robin) boundary condition, where h_{ij} denotes the convective heat transfer coefficient for a specific process step i and pipe dimension j and u_{a_i} the ambient temperature.

$$\begin{aligned} \text{BC2: } \frac{\partial u}{\partial r} &= -h_{ij}(u - u_{a_i}), \text{ at } r = r_{out} \\ &\forall i = 1 \dots n_s \text{ and } \forall j = 1 \dots n_d \end{aligned} \tag{6}$$

Since the investigated pipe production line consists of nine cooling and conditioning steps ($n_s = 9$) and several pipe dimensions ($n_d > 1$), the total number of unknown heat transfer coefficients is $n_h = n_s \times n_d$.

In well-defined settings, the relationship between problem dimension (characteristic length, l_j), heat transfer coefficient and thermal conductivity of the surrounding fluid λ_{F_i} can be described by the Nusselt number Nu_i [24].

$$\text{Nu}_i = \frac{h_{ij} l_j}{\lambda_{F_i}}, \; \forall i = 1 \dots n_s \text{ and } \forall j = 1 \dots n_d \tag{7}$$

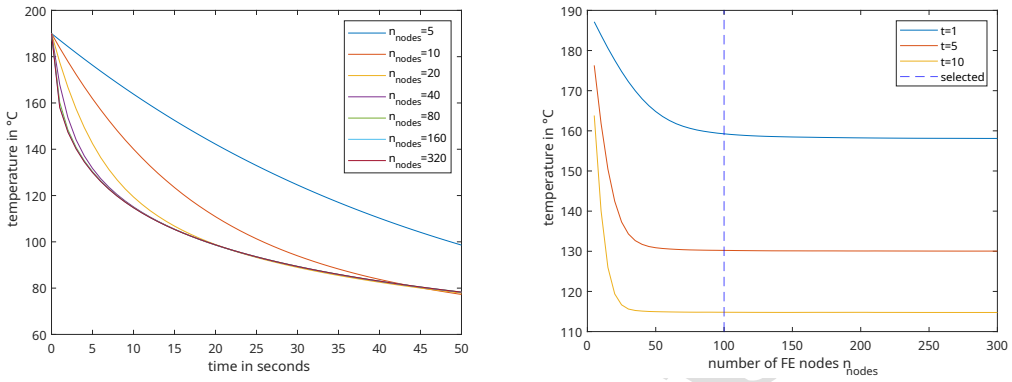

(a) Outer surface temperature over time for spatial resolutions (n_{nodes}). (b) Outer surface temperature over spatial resolution at different times.

Figure 3: Grid independence study at $r = r_{out}$ to determine an appropriate mesh size (dashed line) of the FE model.

The Nusselt number is determined as empirical correlation based on Prandtl number Pr_i and Reynolds number Re_i for forced convection or Grashof number Gr_i for natural convection.

$$\mathrm{Nu}_i = \begin{cases} f(\mathrm{Re}_i, \mathrm{Pr}_i), \text{forced convection} \\ f(\mathrm{Gr}_i, \mathrm{Pr}_i), \text{natural convection} \end{cases} \tag{8}$$

Even though λ_{F_i} is known for water and air at different temperatures, the characteristic length and the function for computing Nu_i are largely unknown, apart from problems with limited complexity [6]. As a consequence, the proposed method bypasses the need for empirical correlations (8), while still integrating the knowledge of general dependencies (7) to reduce the number of unknown parameters via decomposing the heat transfer coefficients (see below).

3. Methodology

The proposed methodology consists of four main steps. First, a high-fidelity FE model generates randomized data in an appropriate parameter range. Second, a small number of basis functions are extracted via POD, which cover the main dynamics of the system. Third, the governing heat equation is projected on these basis functions via the Galerkin method to build a ROM. Finally, the unknown heat transfer coefficients are identified and validated on simulated and experimental data from an actual production line.

3.1. Grid Independence Study for Finite Element Model

To extract the main dynamics via the POD, a high-fidelity FE model is created based on aforementioned equations for heat transfer (1), initial condition (4) and boundary conditions (5, 6). The FE model is implemented via the Matlab pdepe function which relies on the ode15 solver to dynamically choose appropriate time steps for temporal integration. The nonlinear thermal diffusivity $\alpha(u)$ is updated at each time step according to the temperature u. A decisive factor for the accuracy of the FE model is the number of nodes n_{nodes} (elements) in the mesh and therefore its DOF to approximate the spatial domain. In general, finer mesh sizes improve the accuracy, whereas diminishing returns are expected leading to a trade-off between model complexity and accuracy. To determine a suitable number of nodes, a grid independence study is performed [10, 16] where the nodes are uniformly distributed along the radial direction.

Since an adiabatic boundary on the inside is assumed, large temperature gradients in radial direction are only expected close to the outer surface of the pipe, particularly at the beginning of the line. Therefore, as shown in Fig. 3, the grid independence study is performed for temperatures on the outer surface $r = r_{out}$.

All simulation runs were initialized with $u_0 = 190$ °C with a simulated duration of 50 seconds. As depicted in Fig. 3a for different n_{nodes} with linear shape functions, the simulated outer surface temperature differs significantly at the beginning and approach similar values after 50 seconds (apart from $n_{nodes} = 5$). Consequently, the first seconds are crucial for selecting a sufficient number of FE-nodes, which is shown in detail in Fig. 3b. The outer surface temperature for different points in time show that a resolution of $n_{nodes} = 100$ approximate the spatial domain accurately from the beginning.

The selected number of FE-nodes is used to generate input (train) data X_j for the POD for all n_d pipe dimensions. Additionally, a test data set is generated to validate the approximation capabilities of the resulting ROM. Both data sets are generated with 60 randomized steps lasting 60 seconds each, where the ambient temperature u_a (20-

80 °C) and convective heat transfer coefficient h (1-1500 $W/(m^2K)$) are drawn uniformly to cover a wide range of dynamical behavior [25].

3.2. Proper Orthogonal Decomposition

The underlying assumption of a POD is that the behavior of many dynamical systems can be accurately approximated by a few dominant patterns. To extract these patterns the singular vector decomposition (SVD) is used, where a given matrix $X \in \mathbb{R}^{n\times m}$ is decomposed into a matrix of left singular vectors $U \in \mathbb{R}^{n\times n}$, a diagonal matrix $\Sigma \in \mathbb{R}^{n\times m}$ consisting of singular values σ_i and a matrix of right singular vectors $V^T \in \mathbb{R}^{m\times m}$.

$$X = U\Sigma V^T \tag{9}$$

The column vectors in U represent the optimal spatial basis functions ϕ_p (POD modes) listed in descending order.

$$U = \begin{bmatrix} | & | & | & | \\ \phi_1 & \phi_2 & \dots & \phi_n \\ | & | & | & | \end{bmatrix} \tag{10}$$

Consequently, the characteristic of the SVD ensures, that selecting the first n_p basis functions leads to an optimal matrix approximation [26, 27]. As shown in Fig. 4 for the first 10 singular values for the input (train) data X_j (described above) of one pipe dimension j, the cumulative normalized value $\sum_{p=1}^{n_p}\sigma_p / \sum_{p=1}^{n}\sigma_p$ quickly increases to over 99 % approximation capabilities. The resulting spatial POD modes associated with the first 4 singular values are depicted in Fig. 5. The POD modes are determined for each pipe dimension separately and are constant over time and independent of $\alpha(u)$.

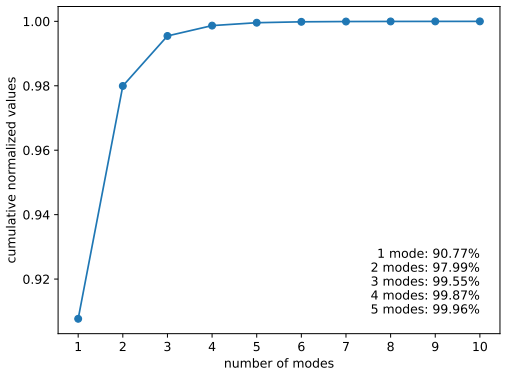

Figure 4: Cumulated normalized singular values determined by the POD for the input (train) data X_j of one pipe dimension j.

3.3. Galerkin Method

To project the governing equation, the Galerkin method is applied where the heat equation (1) is multiplied with

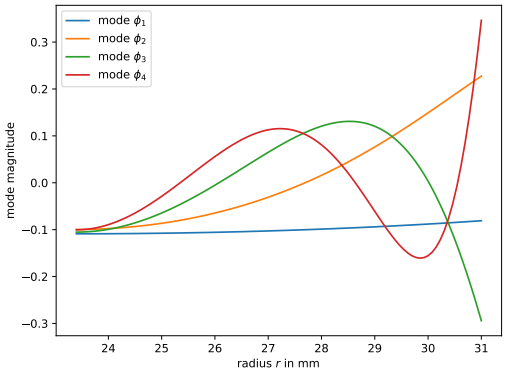

Figure 5: Spatial basis functions $\phi_p(r)$ determined by the POD for the input (train) data X_j of one pipe dimension j.

optimal POD basis functions ϕ_p and integrated over the entire 1d spatial domain $[r_{in}, r_{out}]$.

$$\int_{r_{in}}^{r_{out}} \phi_p \frac{\partial u}{\partial t} dr - \int_{r_{in}}^{r_{out}} \phi_p \frac{\alpha}{r}\frac{\partial u}{\partial r} dr - \int_{r_{in}}^{r_{out}} \alpha\phi_p \frac{\partial^2 u}{\partial r^2} dr = 0,\ \forall p = 1 \dots n_p \tag{11}$$

To account for boundary conditions, Green's first identity is used, which results in an integration term over the boundary Γ and the radial domain $[r_{in}, r_{out}]$ respectively.

$$\int_{r_{in}}^{r_{out}} \alpha\phi_p \frac{\partial^2 u}{\partial r^2} dr = \int_{\Gamma} \alpha\phi_p \frac{\partial u}{\partial r} d\Gamma - \int_{r_{in}}^{r_{out}} \frac{\partial \alpha\phi_p}{\partial r}\frac{\partial u}{\partial r} dr \tag{12}$$

To explicitly include the boundary conditions in the ROM, the integration over Γ is solved and substituted into (11).

$$\int_{r_{in}}^{r_{out}} \phi_p \frac{\partial u}{\partial t} dr - \int_{r_{in}}^{r_{out}} \phi_p \frac{\alpha}{r}\frac{\partial u}{\partial r} dr + \int_{r_{in}}^{r_{out}} \frac{\partial \alpha\phi_p}{\partial r}\frac{\partial u}{\partial r} dr + \alpha(r_{out})\phi_p(r_{out})h[u(r_{out}) - u_a] = 0 \tag{13}$$

To discretize the time domain the implicit Euler backward method is formulated based on a temporal step size Δt.

$$\frac{\partial u}{\partial t} \approx \frac{u(t+\Delta t) - u(t)}{\Delta t} \tag{14}$$

Additionally, an approximation function u_h is defined for $u(r, t+\Delta t)$, where n_p denotes the number of basis functions ϕ_q and a_q the time dependent coefficient.

$$u(r, t+\Delta t) \approx u_h = \sum_{q=1}^{n_p} a_q(t+\Delta t)\phi_q \tag{15}$$

Substituting the approximation function u_h into (13) yields the Galerkin approximation in discretized form.

$$\int_{r_{in}}^{r_{out}} \phi_p \sum_{q=1}^{n_p} a_q(t+\Delta t)\phi_q dr - \Delta t \int_{r_{in}}^{r_{out}} \phi_p \frac{\alpha}{r} \sum_{q=1}^{n_p} a_q(t+\Delta t)\frac{d\phi_q}{dr} dr + \Delta t \int_{r_{in}}^{r_{out}} \frac{d\alpha\phi_p}{dr} \sum_{q=1}^{n_p} a_q(t+\Delta t)\frac{d\phi_q}{dr} dr + \Delta t\alpha(r_{out})\phi_p(r_{out})h \sum_{q=1}^{n_p} a_q(t+\Delta t)\phi_q(r_{out}) - \int_{r_{in}}^{r_{out}} \phi_p u(t) dr - \Delta t\alpha(r_{out})\phi_p(r_{out})hu_a = 0, \quad \forall p = 1 \dots n_p \tag{16}$$

Extracting the unknown coefficients $a(t+\Delta t)$ leads to a system of linear equations to be solved for $\vec{a} \in \mathbb{R}^{n_p}$ in each time step, representing the reduced order model with n_p degrees of freedom.

$$A\vec{a} = b \tag{17}$$

The entries of matrix A are constructed as follows.

$$A_{pq} = \int_{r_{in}}^{r_{out}} \phi_q\phi_p dr - \int_{r_{in}}^{r_{out}} \phi_p \frac{\alpha}{r}\frac{d\phi_q}{dr} dr + \Delta t \int_{r_{in}}^{r_{out}} \frac{d\alpha\phi_p}{dr}\frac{d\phi_q}{dr} dr + \Delta th\alpha(r_{out})\phi_p(r_{out})\phi_q(r_{out}) \quad \forall p, q \in [1, n_p] \tag{18}$$

Furthermore, the entries of b are determined by the following equation.

$$b_p = \int_{r_{in}}^{r_{out}} \phi_p \sum_{q=1}^{n_p} a_q(t)\phi_q dr + \Delta th\alpha(r_{out})\phi_p(r_{out})u_a, \; \forall p = 1 \dots n_p \tag{19}$$

To select a suitable number n_p of basis functions ϕ_p, the mean absolute percentage error (MAPE) is evaluated over the number of time steps n_t and spatial nodes n_{nodes} for each n_p.

$$\text{MAPE}_{n_p} = \frac{1}{n_t \; n_{nodes}} \sum_{i}^{n_{nodes}} \sum_{j}^{n_t} \left| \frac{u(r_i, t_j) - \hat{u}(r_i, t_j)}{u(r_i, t_j)} \right| \tag{20}$$

The simulated temperatures from the high-fidelity FE model and its approximation from the ROM are denoted by $u(r,t)$ and $\hat{u}(r,t)$ respectively. The resulting MAPE scores based on $\Delta t = 1$ for train and test data sets are shown in Fig. 6. Due to the wide range of parametric variations in the POD input data (train), the ROM approximates both data sets similarly well. Additionally, using a long simulation time of 3600 seconds for the validation ensures that the ROM does not diverge within the relevant time span. Consequently, $n_p = 4$ POD modes and $\Delta t = 1$ are selected for the parameter identification, which reduces the DOF by a factor of 25 (96 %) while maintaining high accuracy with a MAPE score of 0.11 % (train) and 0.13 % (test) in comparison to the high-fidelity FE model. Additionally, the number of arithmetic operations to solve the system of equations (17) is reduced by 94.4 % from 496 to 28.

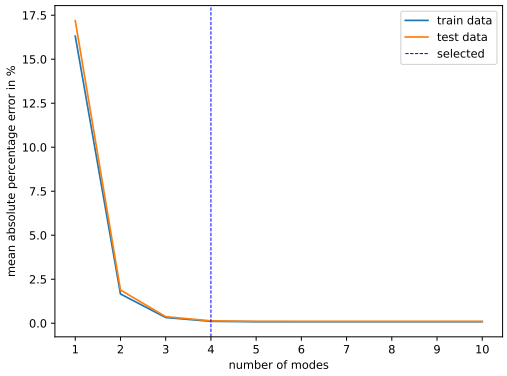

Figure 6: Mean absolute percentage error for approximating the train (POD input) and test data via the Galerkin method over the entire spatial and time domain for one pipe dimension j.

3.4. Parameter Identification

To identify the convective heat transfer coefficients of the outer boundary condition, the identification procedure relies on temperature measurements along the production line. The problem domain consists of $n_s = 9$ cooling and conditioning steps and n_d different pipe dimensions, leading to an $H^{n_s \times n_d}$ matrix of n_h unknown coefficients.

$$H = \begin{bmatrix} h_{11} & \dots & h_{1n_d} \\ & \vdots & \\ h_{n_s 1} & \dots & h_{n_s n_d} \end{bmatrix} \tag{21}$$

Fundamentally, the optimization problem can be formulated where the optimal parameters in H must be identified to minimize a loss function $\mathcal{L}$.

$$H^* = \arg\min_H \mathcal{L} \tag{22}$$

To reduce the number of unknown parameters and integrate the dependencies described by the Nusselt number, the matrix H can be decomposed, where each element h_{ij} is determined as a function of component-specific Nusselt number Nu_i, fluid-specific thermal conductivity λ_{F_i} and dimension-specific characteristic length l_j.

$$h_{ij} = \frac{\text{Nu}_i \lambda_{F_i}}{l_j}, \forall i = 1 \dots n_s \text{ and } \forall j = 1 \dots n_d \tag{23}$$

As a consequence, the optimization problem is restated in terms of Nu_i and l_j (λ_{F_i} is known for air and water) through substituting (23) into subsequent loss functions. Therefore, instead of n_s times n_d unknown parameters, only $n_s + n_d$ parameters need to be identified, reducing the problem complexity from quadratic to linear.

To find a solution to this optimization problem, the sum of squared errors is used as data loss function $\mathcal{L}_{\mathrm{data}}$ where the temperature measurements $u(r_{out}, t_m)$ on the outer surface $r = r_{out}$ at sparse points in time t_m and the output of the ROM $\hat{u}(r_{out}, t_m)$ for n_d pipe dimensions and n_m measurement points (sensors) are compared.

$$\mathcal{L}_{\mathrm{data}} = \sum_{j=1}^{n_d} \sum_{k=1}^{n_m} (u(r_{out_j}, t_{m_k}) - \hat{u}(r_{out_j}, t_{m_k}))^2 \tag{24}$$

However, uniqueness of the solution is not guaranteed due to the ill-posed nature of the IHTP, which might even lead to physically infeasible solutions. Consequently, we propose to extend the loss function with a lower boundary $h_{ij} \geq 0$ as positivity constraint, a l_2 regularization [4] and well-known relative constraints to improve the convergence of the identification process.

First, to ensure physically feasible coefficients, a loss term $\mathcal{L}_{\mathrm{pos}}$ is added to enforce positive heat transfer coefficients, where λ_{pos} specifies the weight of constraint violations defined by the slack variable l_{pos_i}.

$$\mathcal{L}_{\mathrm{pos}} = \sum_{i=1}^{n_s} (\lambda_{\mathrm{pos}} l_{\mathrm{pos}_i})^2 \tag{25}$$

$$l_{\mathrm{pos}_i} = \begin{cases} \sum_{j=1}^{n_d} (h_{ij}), & \text{if } h_{ij} < 0 \\ 0, & \text{otherwise} \end{cases} \tag{26}$$

Second, l_2 regularization (also known as Tikhonov regularization) is applied to penalize large coefficients and ease the identification process [4, 11]. Therefore, the l_2 loss function $\mathcal{L}_{l_2}$ is determined by the sum of squared and weighted (λ_{l_2}) values over all heat transfer coefficients.

$$\mathcal{L}_{l_2} = \sum_{i=1}^{n_s} \sum_{j=1}^{n_d} (\lambda_{l_2} h_{ij})^2 \tag{27}$$

Third, while simultaneously considering multiple cooling and conditioning steps increases the level of complexity, it also provides a rich source of information. In particular, since it is possible to define relative constraints based on the process steps given in Tab. 1:

- h of mixed convection $<$ h of forced convection, provided that the same fluids are involved: $h_4, h_6, h_9 < h_7$
- h of air based convection $<$ h of water based convection, due to higher thermal conductivity of water: $h_7 < h_2$
- h of immersion cooling $<$ h of spray cooling: $h_2 < h_1, h_3, h_5, h_8$

Even though these constraints could be enforced via carefully chosen individual λ_{l_2} weights for each coefficient, it proves to be cumbersome and is prone to subjective influence. Alternatively, a discontinuous constraint function, similar to the positivity constraint, could be imposed where coefficients are significantly penalized as soon as a constraint is violated. However, the discontinuity of the loss function causes issues in the convergence, due to mutually constraining coefficients moving back and forth during the identification.

In contrast to that, we propose to use soft constraints, implemented via logistic functions to enforce relative constraints. The midpoint of the logistic function is defined as the constraining coefficient on the upper boundary h_u. Additionally, to ensure that the growth rate of the function remains meaningful over different coefficient magnitudes, it is adaptively calculated based on the current absolute value of h_u and a fixed parameter k which is experimentally selected. The loss term for each mutually constraining pair of coefficients is defined as follows,

$$l_{\mathrm{rel}}(h_u, h_l) = \frac{1}{1 + exp\left(-(h_l - h_u)\frac{k}{abs(h_u)}\right)}, \tag{28}$$

where $h_l < h_u$ is imposed.

Consequently, the overall loss term for relative constraints $\mathcal{L}_{\mathrm{rel}}$ is computed as the sum of squared constraint violations l_{rel}, where λ_{rel} specifies the weight of the constraints.

$$\mathcal{L}_{\mathrm{rel}} = \sum (\lambda_{\mathrm{rel}} l_{\mathrm{rel}})^2 \tag{29}$$

Adding each loss term leads to an overall loss function which addresses the ill-posed nature of the IHTP and enables a robust identification of heat transfer coefficients in spite of sparse and noisy measurements in the time domain.

$$H^* = \arg\min_H \left(\mathcal{L}_{\mathrm{data}} + \mathcal{L}_{\mathrm{pos}} + \mathcal{L}_{l_2} + \mathcal{L}_{\mathrm{rel}}\right) \tag{30}$$

To solve this optimization problem, a wide range of algorithms is available [4], whereas the Levenberg-Marquardt (LM) algorithm is selected as a gradient-based approach well-suited for nonlinear problems [8, 22].

4. Simulation Results

To validate the proposed methodology, simulated as well as experimental temperature measurements are used. The general simulation setup, the identifiability of coefficients and the effect of relative constraints and l_2 regularization are described in the following subsections.

4.1. Simulation Setup

A simulation run, meaning following one cross-section of the pipe through the entire production line, requires parameters and model inputs, where parameters are inherent to the system or pipe dimensions and inputs can vary for each production (simulation) run. The parameters of the system are aligned with the actual production line and material. Consequently, $n_s = 9$ cooling and conditioning steps as well as different pipe dimensions (r_{in}, r_{out}) are considered. Additionally, the density and thermal conductivity of PVC are $\rho = 1400\ kg/m^3$ and $\lambda_S = 0.17\ W/(mK)$ respectively while the temperature dependent heat capacity is given in (3).

The simulation results for one exemplary production run and pipe dimension according to the actual settings (see Fig. 1 and Tab. 1) with known initial temperature u_0 and ambient temperature u_{a_i} are shown in Fig. 7. Importantly, each discontinuity in the outer pipe temperature marks the entrance into a new process step with potentially different ambient temperature (u_a, green line) and coefficients which were arbitrarily chosen in $W/(m^2K)$ for this exemplary simulation run:

$$h = [1250, 750, 2000, 100, 2500, 100, 300, 1250, 25]$$

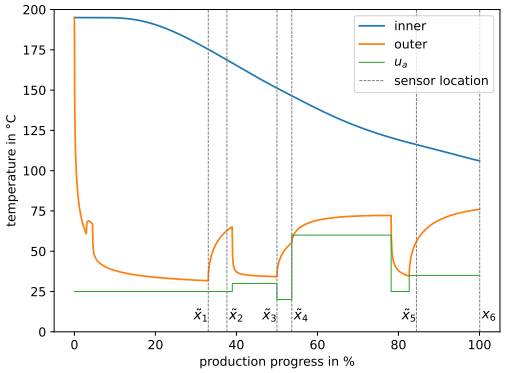

Figure 7: Inner and outer pipe wall temperature for one exemplary simulation run with manual $\tilde{x}_k$ and fixed (x_6) sensors corresponding to the actual production process.

In addition to the resulting temperatures, Fig. 7 shows the position of manual $\tilde{x}_k$ and fixed sensors x_k corresponding to the production process. Depending on the production speed v_{x_j} and sensor locations, temperature measurements are collected at $t = t_{m_k} = x_k/v_x$. In this regard x_6 corresponds to the fixed temperature sensor at the end of the cooling and conditioning part (see Fig. 1). Furthermore, the sensors at $\tilde{x}_k \forall k < 6$ indicate the position of manual temperature measurements in partially open process steps.

The radial temperature distributions from inner r_{in} to outer r_{out} radius at four sensor locations are depicted in Fig. 8. As shown, while the pipe is moving through the line, the temperature gradient flattens out from the start $x = 0$ to the end of the line at x_6.

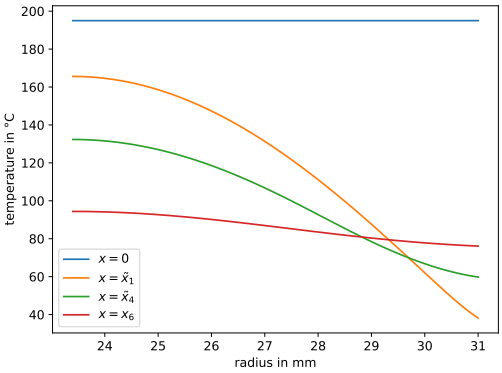

Figure 8: Radial temperature distributions $u(r, t_{m_k})$ at four sensor locations for one pipe dimension j.

The described simulation setup is used to analyze the identifiability of coefficients with limited measurements and the effect of l_2 regularization and relative constraints.

4.2. Identifiability of Heat Transfer Coefficients

To determine the general identifiability of heat transfer coefficients with limited measurements, the Sobol global sensitivity method is used [28]. In contrast to a local sensitivity analysis, for instance based on the Jacobian matrix, the global sensitivity contains information about the entire problem space.

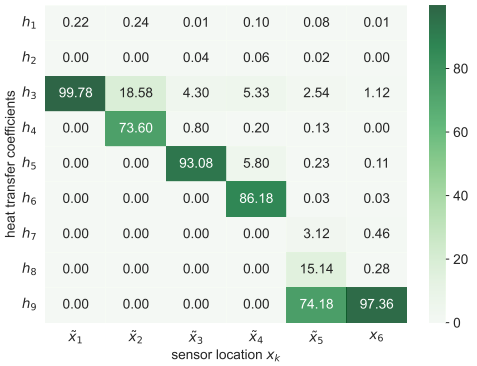

Figure 9: First order Sobol sensitivity indices for each unknown heat transfer coefficient h_i and sensor location ($\tilde{x}_k$, x_k).

In this case, the Sobol sensitivity relies on a Monte Carlo simulation with varying parameter values to com-

pute the sensitivity indices based on the temperature variance in each sensor location. The resulting first order indices for all coefficients h_i and sensor locations ($\tilde{x}_k$, x_k) are column-wise normalized as shown in Fig. 9.

These indices can be interpreted as global identifiability information when a specific sensor is available. For instance, the sensor measurements at $\tilde{x}_2$ contain a significant amount of information about h_3 and h_4. Therefore, these coefficients are easier to identify given the sensor at location $\tilde{x}_2$ in comparison to the other coefficients. As shown, since only six manual and fixed sensor locations are accessible in the actual production process some coefficients (h_1, h_2, h_7, h_8) are difficult to identify, proving the need for additional considerations to address the ill-posed nature.

4.3. Monte Carlo Analysis

To determine the effect of relative constraints and l_2 regularization, a Monte Carlo (MC) simulation with $n_{mc} = 100$ randomized repetitions is performed for the unconstrained (only positivity is enforced via $\lambda_{\text{pos}} = 100$) and constrained ($\lambda_{l_2} = 10^{-4}$, $\lambda_{\text{rel}} = 2$, $k = 10$) identification procedure For this purpose, one simulated production run with arbitrary coefficients provides the target temperature measurements for all six sensor locations. To randomize the repetitions, a Gaussian noise e is added to the target output, where the standard deviation $std(e)$ is computed with a signal-to-noise ratio (SNR) of 100 leading to an added noise of 1 % with regard to the simulated temperature $u(r_{out}, t_{m_k})$ at each sensor location x_k.

$$\text{SNR} = \frac{u(r_{out}, t_{m_k})}{std(e)} \tag{31}$$

Additionally, to analyze the robustness of the proposed identification procedure, the initial parameter guesses for Nusselt numbers Nu_{i_0} and characteristic length l_{j_0} are randomly drawn for each repetition from an uniform distribution ranging from $0 - 100$ and $0 - r_{out}$ respectively.

As a result, while the unconstrained procedure only identifies coefficients accurately when the Sobol indices are high (see Fig. 9), the proposed loss function increases the overall identifiability and accurately identifies two more coefficients (h_7, h_8) as shown in Fig. 10. Even though the first two coefficients (h_1, h_2) are still difficult to identify, the proportions are similar to the actual coefficients, in contrast to the unconstrained identification procedure showing the effectiveness of the proposed methodology.

5. Experimental Results

After validating the general effectiveness of the proposed methodology with simulated data, the applicability and properties of the identification procedure are analyzed on experimental temperature measurements.

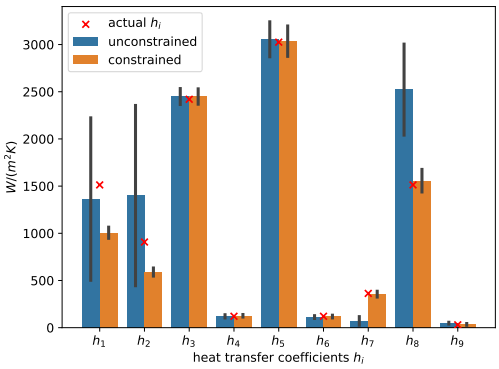

Figure 10: Identified coefficients with mean values (bar height) and standard deviation (+/- σ) resulting form a Monte Carlo simulation for randomized unconstrained and constrained identification procedures.

5.1. Experimental Setup

As shown in Fig. 1, the line consists of 9 cooling and conditioning steps with different lengths and characteristics. The PVC temperature in the die head is measured via a thermocouple sensor directly within the material, representing the initial condition of the ROM. Moreover, at the end of step 9, an infrared temperature sensor is mounted above the moving pipe and continuously measures the outer surface temperature (see Fig. 11) at the location x_6.

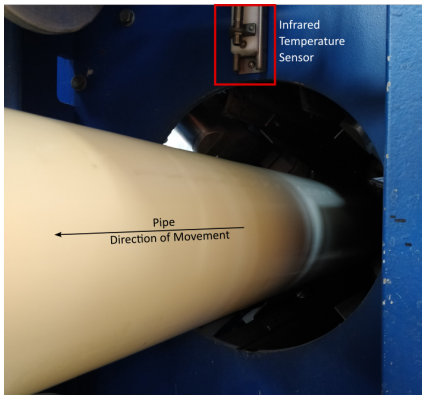

Figure 11: Infrared temperature sensor providing continuous measurements at the end of the cooling and conditioning process at x_6.

To ease the parameter identification and validation, additional manual measurements were performed with a handheld infrared thermometer at $\tilde{x}_k$ in all process steps where the pipe surface is at least partially accessible (see Fig. 1 and 7). To improve the robustness of manual mea-

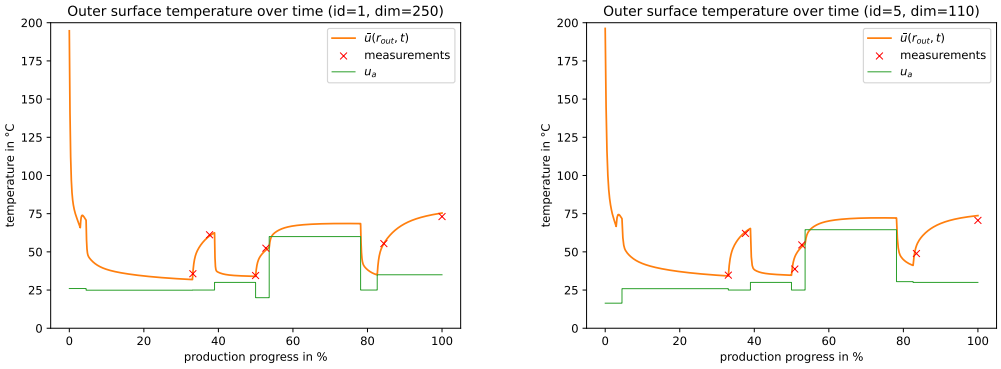

Figure 12: Simulation results of cooling and conditioning steps with identified parameters, where the production run on the left was used during identification.

surements, 10 consecutive measurements are performed for each sensor location at an interval of 10 seconds. These measurements were performed for three different production runs (1, 5, 10) and two dimensions. The resulting mean target temperatures for both manual and automated measurements are shown in Tab. 2.

Run Id	$\tilde{x}_1$	$\tilde{x}_2$	$\tilde{x}_3$	$\tilde{x}_4$	$\tilde{x}_5$	x_6
1 (250mm)	35.7	61.2	34.5	52.4	55.4	73.1
2 (110mm)	-	-	-	-	-	73.6
3 (160mm)	-	-	-	-	-	74.1
4 (315mm)	-	-	-	-	-	69.2
5 (110mm)	34.8	62.1	38.8	54.6	48.9	70.6
6 (110mm)	-	-	-	-	-	74.8
7 (110mm)	-	-	-	-	-	74.3
8 (315mm)	-	-	-	-	-	68.4
9 (250mm)	-	-	-	-	-	73.5
10 (110mm)	34.1	61.0	45.1	52.2	56.7	77.2
11 (160mm)	-	-	-	-	-	74.4

Table 2: Manual ($\tilde{x}_k$) and automated (x_6) temperature measurements collected from different production runs (id) and dimensions used for parameter identification and validation.

5.2. Identification with Experimental Data

The measurements in Tab. 2 are used to validate the proposed methodology for parameter identification based on a ROM with 4 spatial modes. For that purpose, the data from 4 production runs (1, 3, 4, 10) are used in the identification to minimize the loss function (30) with the Levenberg-Marquardt optimization algorithm. Since $n_d = 4$ pipe dimensions and $n_s = 9$ process steps are considered, the number of unknown convective heat transfer coefficients h_{ij} amounts to 36 which are decomposed in 9 Nusselt numbers and 4 characteristic lengths representing 13 unknown parameters for the identification procedure.

To demonstrate the robustness of the parameter identification, 100 repetitions with randomized initial parameter guesses for Nusselt number $(0 - 100)$ and characteristic length $(0 - r_{out_j})$ are performed. For regularization purposes, $\lambda_{\text{pos}} = 100$ for the positivity constraint, $\lambda_{l_2} = 2 \times 10^{-4}$ to promote smaller coefficients and $\lambda_{\text{rel}} = 2$ as well as $k = 10$ to enforce aforementioned relative constraints were chosen.

The resulting heat transfer coefficients over 100 randomized identification procedures is shown in Fig. 13 for one pipe dimension. The coefficients are consistently identified with a mean variance $\bar{\sigma}^2$ of 1.4×10^{-3} and physically feasible. Even though the absolute values of h_i vary between pipe dimensions depending on the identified characteristic length, the proportions remain the same.

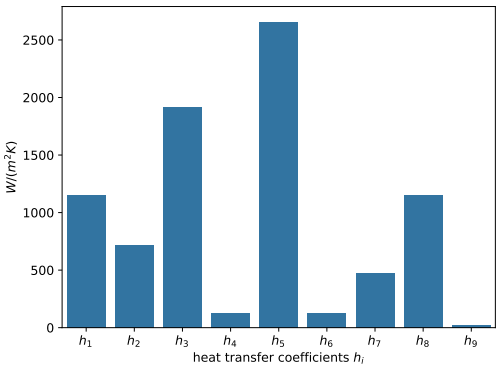

Figure 13: Identified mean heat transfer coefficients h_i for a 250mm pipe over 100 randomized repetitions.

The resulting simulated outer surface temperature at

$r = r_{out}$ with the identified mean coefficients in comparison with available temperature measurements are shown in Fig. 12 for two production runs with manual measurements. As can be seen, the simulation provides a good fit for measurements which were used during the identification (left) and the others which were not used (right) with a MAPE score of 1.5 % (train) and 4.9 % (test) respectively. The difference in the train and test scores is mainly caused by two manual measurements during one production run (id 5) at the locations $\tilde{x}_3$ and $\tilde{x}_5$, which can be explained by large temperature gradients in these areas and therefore, a high sensitivity to small variations during manual measurements.

5.3. Convergence Analysis

Apart from accurate results, an important aspect of every identification method is its convergence behavior. In particular when the initial parameter guesses have a wide range due to unknown absolute values. In the case above, the initial guesses for the Nusselt number (0-100) and characteristic length (0-r_{out}) effectively lead to a range from 0 to ∞ for the initial coefficients h_{ij} in H. Additionally, relative constraints are not enforced during the random generation of initial guesses leading to constraint violations at the beginning of the parameter identification.

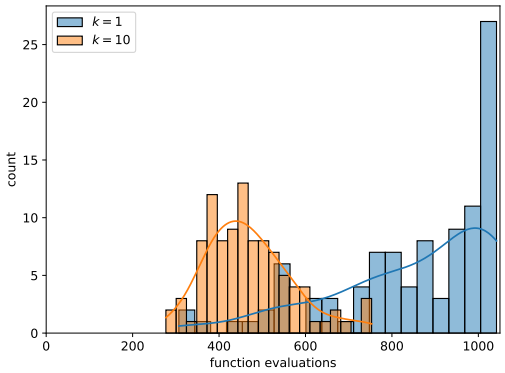

Figure 14: Analysis of required function evaluations to converge to a local minimum over 100 randomized repetitions for two values of k, see (28), where $k = 10$ was used during identification and the maximum number of function evaluations was limited to 1000.

In spite of these difficulties, the proposed methodology based on positivity constraints, relative constraints and l_2 regularization with corresponding weights and settings (see above) requires on average 470 function evaluations over 100 randomized repetitions. Importantly, the number of function evaluations of the loss function include evaluations required to numerically approximate the Jacobian matrix used by the Levenberg-Marquardt optimization algorithm. As shown in Fig. 14 for $k = 10$ (28), the number of function evaluations closely resembles a normal distribution, where 800 or more evaluations are highly unlikely. However, the growth rate for the soft constraints must be chosen carefully due to its impact on the convergence behavior, as depicted by $k = 1$ in Fig. 14.

5.4. Approximation Error

In addition to the general quality and convergence behavior of the identification, the error caused by approximating the high-fidelity FE model is analyzed. For that purpose, the identified mean heat transfer coefficients are used to simulate production run 1 (see Tab. 2) with the FE model. The results are used as basis for computing the MAPE (20) over the entire time and spatial domain for a range of POD modes.

Similar to the synthetic validation conducted during the development of the ROM (see Fig. 6), the MAPE decreases rapidly from 40 % to below 1 %. However, using the identified coefficients generally results in higher relative errors when compared to the synthetic results. This might be caused by the limited range (0-1500) of coefficients used for the POD mode generation in contrast to coefficients beyond 1500 $W/(m^2K)$ encountered during the identification procedure. For instance, using 4 POD modes increases the MAPE from 0.1 % to 0.3 %, which is still practically acceptable due to a significant reduction of model complexity and execution time when compared to the high-fidelity model.

5.5. Effect of Identification Settings

To analyze the effect of l_2 regularization, relative constraints, and their settings (weights and growth rate), 100 randomized identification procedures were performed for different configurations. Each identification procedure was limited to 1000 function evaluations, since appropriate settings usually require far less iterations, as shown before.

The settings and results are summarized in Tab. 3, where λ_{l_2}, λ_{rel} and k represent the configuration for the weights of l_2 regularization and relative constraints as well as the growth rate for the soft constraints. Moreover, the fourth column indicates how many repetitions converged within 1000 function evaluations, whereas the MAPE score is provided separately for train (production runs 1, 4, 5, 8) and test data sets. In addition to the convergence rate and MAPE scores, essential aspects of the identification are the number of repetitions that resulted in violated positivity $h_i > 0$ and relative constraints $h_l > h_u$ as well as the mean variance over all identified coefficients $\bar{\sigma}^2(h)$.

As shown in Tab. 3, the settings used during the experimental validation (id 1) lead to a convergence rate of 100 % with acceptable MAPE scores and no constraint violations. Reducing the growth rate to $k = 5$ (id 2) or $k = 1$ (id 3, see Fig. 14) or removing the l_2 regularization (id 4) leads to worse convergence behavior and a high variance in identified coefficients. In contrast to that, ignoring the relative constraints (id 5) does not affect the convergence

	Settings				MAPE in %		Violations		
Id	λ_{l_2}	λ_{rel}	k	Converged	Train	Test	$h_i > 0$	$h_l < h_u$	$\bar{\sigma}^2(h)$
1	2×10^{-4}	2.0	10	100	1.46	4.89	0	0	1.4×10^{-3}
2	2×10^{-4}	2.0	**5**	99	1.49	4.81	1	1	2.0×10^{3}
3	2×10^{-4}	2.0	**1**	71	1.52	4.81	2	2	4.5×10^{3}
4	**0.0**	2.0	10	24	2.33	4.35	4	1	1.7×10^{12}
5	2×10^{-4}	**0.0**	-	100	1.44	4.99	100	0	2.3×10^{-2}
6	**0.0**	**0.0**	-	100	1.32	5.08	100	0	8.5×10^{13}

Table 3: Effect of l_2 regularization and relative constraints on convergence rate, mean absolute percentage error (MAPE) and constraint violations (changes to Id 1 are highlighted).

rate, but results in physically infeasible coefficients. Similarly, if neither l_2 regularization nor relative constraints are enforced (id 6), all repetitions converge within 1000 function evaluations, but the resulting coefficients violate physical constraints. Particularly, identified coefficients (h_1, h_2, h_7) with minor identifiability (see above) are infeasible due to values beyond 10^6 $W/(m^2K)$. Consequently, the MAPE score remains similar over different settings, however, convergence and constraint compliance can only be ensured with l_2 regularization and relative constraints.

6. Discussion

Using a ROM based on dominant POD modes reduces the model complexity and therefore, the execution time significantly while maintaining high accuracy which is beneficial for both, parameter identification and subsequent process control and optimization. The proposed methodology was validated with simulated and experimental temperature measurements from a multi-step cooling and conditioning process.

The number of considered POD modes in the ROM and their validity for encountered parameter ranges (e.g. ambient temperatures and coefficients) determine the theoretical lower bound on the approximation error. Consequently, a trade-off must be found between model complexity (execution time) and accuracy where the transitioning phases between process steps are crucial due to high temperature gradients. Similarly, while assumptions regarding the forward model, such as an adiabatic inner boundary or homogeneous ambient conditions along the circumference, can significantly reduce the problem domain, they must be evaluated carefully to avoid large deviations from the actual process.

As clearly shown by the global identifiability analysis, the number and location of temperature sensors have a significant impact on the identifiability of individual heat transfer coefficients. In particular, when two or more process steps are directly connected without any intermediate temperature measurements. In such cases, the ill-posed nature of the IHTP can be successfully addressed by l_2 regularization and relative constraints, as shown by the Monte Carlo analysis for simulated measurements. However, if some process steps have only a minor influence on the production process, the associated coefficients are difficult to identify accurately, while the proposed methodology still keeps the proportions due to relative constraints. Importantly, the influence of each process step is specific to the process and determined by the ambient temperature u_a, length of the process step, temperature difference $u(r_{\text{out}}, t) - u_a$, convection type and fluid in use.

When applied to actual measurements from the pipe extrusion line, the proposed methodology resulted consistently in physically feasible heat transfer coefficients while maintaining a good fit to the measurements. Due to manually measured temperatures with a handheld infrared thermometer some uncertainties are expected regarding the exact measurement point, which can lead to unexplained measurement differences in areas with large temperature gradients. Nevertheless, one key strength of the proposed methodology is its data efficient identification procedure where sparse measurements are sufficient to identify physically sound coefficients for each process step and pipe dimension.

Furthermore, the analysis of the convergence behavior, identification consistency and constraint compliance shows significant improvements in all aspects when applying l_2 regularization and relative constraints. Naturally, the settings (weights λ and growth rate k) of the identification procedure affect the results and must be chosen either manually or automatically [11], whereas both are facilitated by the reduced execution time of the ROM while maintaining high accuracy when compared to the high-fidelity FE model. Similarly, even though the Levenberg-Marquardt optimization algorithm performed well, other algorithms, such as the conjugate gradient method [29], might be considered as well.

7. Conclusion

To effectively control and optimize cooling and conditioning processes in pipe extrusion lines, accurate and computationally efficient models are needed. However, heat transfer coefficients are hardly known for actual production lines and temperature measurements of the pipe surface are only sparsely available in multi-step cooling and conditioning processes leading to an ill-posed inverse heat transfer problem.

To address these challenges a methodology consisting of an efficient reduced order model based on proper orthogonal decomposition and the Galerkin method as well as a constrained parameter identification was proposed. Regarding the latter, l_2 regularization and positivity constraints are enforced in addition to relative constraints to make use of known relationships among cooling and conditioning components. Moreover, to ease the parameter identification a theory-based decomposition of heat transfer coefficients was employed to reduce the number of unknown parameters substantially.

It was shown with simulated and experimental measurements, that the proposed methodology identifies heat transfer coefficients consistently while complying to well-known physical constraints in spite of sparse and noisy temperature measurements. Therefore, the methodology can be successfully and reliably applied to cooling and conditioning processes in pipe extrusion lines and beyond, if the governing equations are known for instance, in pressurized surge lines of nuclear power plants and melting furnaces. Interestingly, extending the parameter identification to material properties (e.g. density, thermal conductivity) or ambient temperatures is straight-forward and the same methods for l_2 regularization and relative constraints can be employed. Furthermore, the resulting reduced order model can not only be applied during parameter identification but also for subsequent process control and optimization due to its computational efficiency.

Apart from this, several research directions for future work were identified. On the one hand, extending the direct model to include the heat conduction in azimuth direction, allows to directly consider varying ambient conditions along the circumference. On the other hand, using automatic differentiation methods, similar to physics-informed neural networks, is expected to reduce the computational effort during identification significantly, since numerical approximation of the derivatives is no longer needed. In addition to that, extending the identification procedure to simultaneously identify heat transfer coefficients, material properties and ambient conditions increases the applicability substantially. Nevertheless, the characteristics of the proposed methodology with its reduced order model, l_2 regularization, relative constraints, and theory-based coefficient decomposition represent the foundation for future work.

Declaration of Competing Interest

The authors declare that they have no known competing financial interests or personal relationships that could have appeared to influence the work reported in this paper.

Acknowledgement

The work presented is part of the project DEEPEN, funded by the Austrian Research Promotion Agency (FFG) under the 41st call of the initiative "Production of the Future", project number 891247 and was supported by Pipelife International GmbH and Pipelife Nederland B.V. as industrial project partners.

References

[1] B.-Y. Wu, Y.-D. Cai, X.-W. Zhao, L. Ye, Construction of pressure-resistance polyethylene-based pipes with highly biaxially oriented structure and self-reinforcing mechanism, Chinese Journal of Polymer Science 41 (2023) 942–955. doi:10.1007/s10118-022-2879-x.

[2] B. P. Wham, C. Argyrou, T. D. O'Rourke, H. E. Stewart, T. K. Bond, Pvco pipeline performance under large ground deformation, Journal of Pressure Vessel Technology 139 (2 2017). doi:10.1115/1.4033939.

[3] R. Hartner, M. Kozek, S. Jakubek, B. Mayer, Gradient boosting regression trees for nonlinear delay identification in a polymer extrusion process, in: 2022 IEEE 21st International Conference on Sciences and Techniques of Automatic Control and Computer Engineering (STA), 2022, pp. 192–197. doi:10.1109/STA56120.2022.10019045.

[4] M. Zálešák, L. Klimeš, P. Charvát, M. Cabalka, J. Kůdela, T. Mauder, Solution approaches to inverse heat transfer problems with and without phase changes: A state-of-the-art review, Energy 278 (9 2023). doi:10.1016/j.energy.2023.127974.

[5] M. M. Billah, A. I. Khan, J. Liu, P. Dutta, Physics-informed deep neural network for inverse heat transfer problems in materials, Materials Today Communications 35 (6 2023). doi:10.1016/j.mtcomm.2023.106336.

[6] S. Cai, Z. Wang, S. Wang, P. Perdikaris, G. E. Karniadakis, Physics-informed neural networks for heat transfer problems, Journal of Heat Transfer 143 (6 2021). doi:10.1115/1.4050542.

[7] J. hang Gu, M. Hong, Q. qing Yang, Y. Heng, A fast inversion approach for the identification of highly transient surface heat flux based on the generative adversarial network, Applied Thermal Engineering 220 (2 2023). doi:10.1016/j.applthermaleng.2022.119765.

[8] P. Duda, A general method for solving transient multidimensional inverse heat transfer problems, International Journal of Heat and Mass Transfer 93 (2016) 665–673. doi:10.1016/j.ijheatmasstransfer.2015.09.029.

[9] M. V. Reddy, B. Hemasunder, S. Ramana, P. R. Babu, P. Thejasree, J. Joseph, State of art on fem approach in inverse heat transfer problems for different materials, Materials Today: Proceedings (7 2023). doi:10.1016/j.matpr.2023.06.323.

[10] T. Lu, W. W. Han, P. X. Jiang, Y. H. Zhu, J. Wu, C. L. Liu, A two-dimensional inverse heat conduction problem for simultaneous estimation of heat convection coefficient, fluid temperature and wall temperature on the inner wall of a pipeline, Progress in Nuclear Energy 81 (2015) 161–168. doi:10.1016/j.pnucene.2015.01.018.

[11] F. Bozzoli, L. Cattani, S. Rainieri, F. S. V. Bazán, L. S. Borges, Estimation of the local heat-transfer coefficient in the laminar flow regime in coiled tubes by the tikhonov regularisation method, International Journal of Heat and Mass Transfer 72 (2014) 352–361. doi:10.1016/j.ijheatmasstransfer.2014.01.019.

[12] G. Palumbo, V. Piglionico, A. Piccininni, P. Guglielmi, D. Sorgente, L. Tricarico, Determination of interfacial heat transfer coefficients in a sand mould casting process using an optimised inverse analysis, Applied Thermal Engineering 78 (2015) 682–694. doi:10.1016/j.applthermaleng.2014.11.046.

[13] Udayraj, K. Mulani, P. Talukdar, A. Das, R. Alagirusamy, Performance analysis and feasibility study of ant colony optimization, particle swarm optimization and cuckoo search algorithms for inverse heat transfer problems, International Journal of Heat and Mass Transfer 89 (2015) 359–378. doi:10.1016/j.ijheatmasstransfer.2015.05.015.

[14] J.-H. Noh, D.-B. Kwak, K.-B. Kim, K.-U. Cha, S.-J. Yook, Inverse heat conduction modeling to predict heat

flux in a hollow cylindrical tube having irregular cross-sections, Applied Thermal Engineering 128 (2018) 1310–1321. doi:10.1016/j.applthermaleng.2017.09.108.

[15] M. Hafid, M. Lacroix, Inverse heat transfer prediction of the state of the brick wall of a melting furnace, Applied Thermal Engineering 110 (2017) 265–274. doi:10.1016/j.applthermaleng.2016.08.162.

[16] M. Gostimirovic, M. Sekulic, M. Trifunovic, M. Madic, D. Rodic, Stability analysis of the inverse heat transfer problem in the optimization of the machining process, Applied Thermal Engineering 195 (8 2021). doi:10.1016/j.applthermaleng.2021.117174.

[17] Z. Malinowski, A. Cebo-Rudnicka, T. Telejko, B. Hadała, A. Szajding, Inverse method implementation to heat transfer coefficient determination over the plate cooled by water spray, Inverse Problems in Science and Engineering 23 (2015) 518–556. doi:10.1080/17415977.2014.923417.

[18] S. Star, G. Stabile, G. Rozza, J. Degroote, A pod-galerkin reduced order model of a turbulent convective buoyant flow of sodium over a backward-facing step, Applied Mathematical Modelling 89 (2021) 486–503. doi:10.1016/j.apm.2020.07.029.

[19] J. Y. Escanciano, A. G. Class, Pod-galerkin modeling of a heated pool, Progress in Nuclear Energy 113 (2019) 196–205. doi:10.1016/j.pnucene.2019.01.017.

[20] L. Jiang, A. Dowling, M.-C. Cheng, Y. Liu, Podtherm-gp: A physics-based data-driven approach for effective architecture-level thermal simulation of multi-core cpus, IEEE Transactions on Computers (2023) 1–12doi:10.1109/TC.2023.3278535.

[21] H. Park, O. Chung, J. Lee, On the solution of inverse heat transfer problem using the karhunen–loève galerkin method, International Journal of Heat and Mass Transfer 42 (1999) 127–142. doi:10.1016/S0017-9310(98)00136-7.

[22] D.-C. Pham, G. Mercère, R. Ouvrard, T. Poinot, Heat equation parameter estimation based on the pod-galerkin approach, IFAC-PapersOnLine 51 (2018) 245–250. doi:10.1016/j.ifacol.2018.09.142.

[23] R. Dahlmann, E. Haberstroh, G. Menges, Menges Werkstoffkunde Kunststoffe, Carl Hanser Verlag GmbH & Co. KG, 2021. doi:10.3139/9783446460867.

[24] M. Kind, A2 Dimensionslose Kenngrößen für die Berechnung von Wärmeübertragern und wärmetechnischen Apparaten, Springer Berlin Heidelberg, Berlin, Heidelberg, 2019, pp. 11–14. doi:10.1007/978-3-662-52989-8_2.

[25] A. Pulimeno, G. Coates-Farley, M. Veresko, L. Jiang, M.-C. Cheng, Y. Liu, D. Hou, Physics-driven proper orthogonal decomposition: A simulation methodology for partial differential equations, MethodsX 10 (2023) 102204. doi:10.1016/j.mex.2023.102204.

[26] S. L. Brunton, J. N. Kutz, Data-Driven Science and Engineering, Cambridge University Press, 2022. doi:10.1017/9781009089517.

[27] M. P. Deisenroth, A. A. Faisal, C. S. Ong, Mathematics for Machine Learning, Cambridge University Press, 2020. doi:10.1017/9781108679930.

[28] I. Sobol', Global sensitivity indices for nonlinear mathematical models and their monte carlo estimates, Mathematics and Computers in Simulation 55 (2001) 271–280. doi:10.1016/S0378-4754(00)00270-6.

[29] F. Bozzoli, S. Rainieri, Comparative application of cgm and wiener filtering techniques for the estimation of heat flux distribution, Inverse Problems in Science and Engineering 19 (2011) 551–573. doi:10.1080/17415977.2010.531466.

Highlights

Title: Addressing Multi-Step Inverse Heat Transfer Problems via Reduced Order Models in a Cooling Process for Polymer Pipes with Sparse Measurements

Authors: Raphael Hartner, Martin Kozek, Stefan Jakubek

- Reduced order model via Galerkin method and proper orthogonal decomposition
- Relative constraints and L_2 regularization to address the ill-posed problem
- Theory-based coefficient decomposition to reduce the number of unknowns
- Validation with an actual production process with multiple product dimensions
- Consistent identification of coefficients despite sparse and noisy measurements

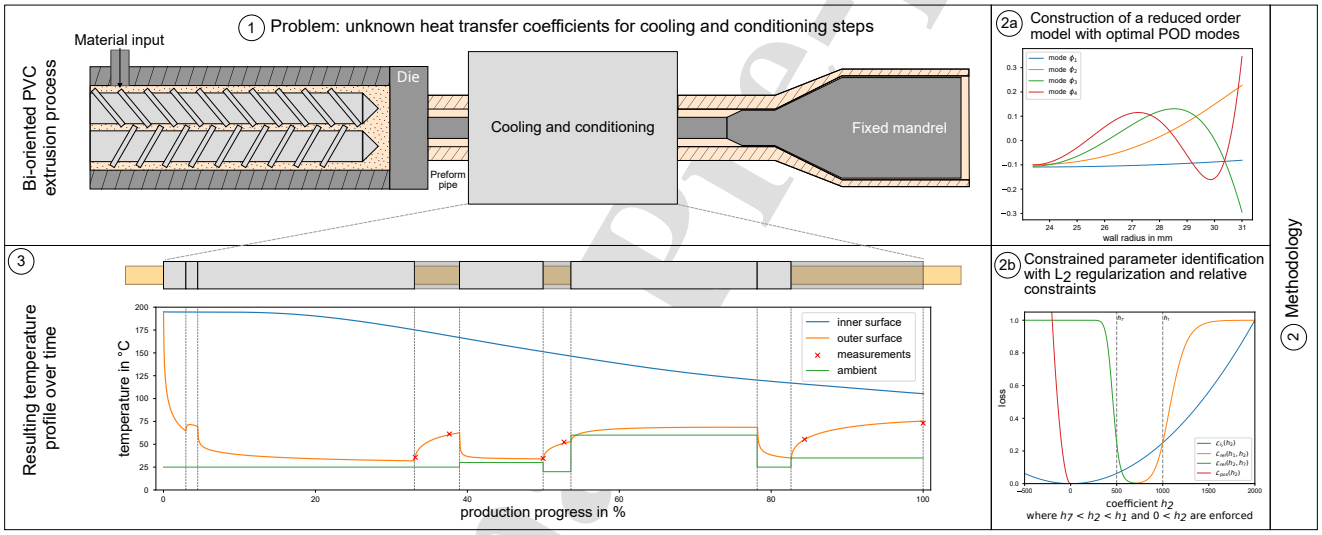

Declaration of interests

☐ The authors declare that they have no known competing financial interests or personal relationships that could have appeared to influence the work reported in this paper.

☒ The authors declare the following financial interests/personal relationships which may be considered as potential competing interests:

Raphael Hartner reports financial support was provided by Austrian Research Promotion Agency (FFG). If there are other authors, they declare that they have no known competing financial interests or personal relationships that could have appeared to influence the work reported in this paper.